Bone 182 (2024) 117055

Contents lists available at ScienceDirect

Bone

journal homepage: www.elsevier.com/locate/bone

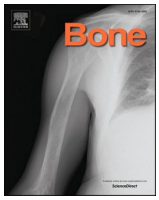

Full Length Article

Chondrocyte hypertrophy in the growth plate promotes stress anisotropy affecting long bone development through chondrocyte column formation

Yuka Yokoyama [a,b], Yoshitaka Kameo [b,c], Junko Sunaga [b], Koichiro Maki [a,b,d,e], Taiji Adachi [a,b,d,e,*]

[a] Department of Micro Engineering, Graduate School of Engineering, Kyoto University, 53 Shogoin-Kawahara-cho, Sakyo-ku, Kyoto, 606-8507, Japan
[b] Department of Biosystems Science, Institute for Life and Medical Sciences, Kyoto University, 53 Shogoin-Kawahara-cho, Sakyo-ku, Kyoto, 606-8507, Japan
[c] Department of Engineering Science and Mechanics, College of Engineering, Shibaura Institute of Technology, 3-7-5 Toyosu Koto-ku, Tokyo, 135-8548, Japan
[d] Department of Mammalian Regulatory Network, Graduate School of Biostudies, Kyoto University, 53 Shogoin-Kawahara-cho, Sakyo-ku, Kyoto, 606-8507, Japan
[e] Department of Medicine and Medical Science, Graduate School of Medicine, Kyoto University, 53 Shogoin-Kawahara-cho, Sakyo-ku, Kyoto, 606-8507, Japan

ARTICLE INFO

Keywords:
Bone development
Growth plate
Chondrocyte column
Continuum-based particle modeling
Computational biomechanics

ABSTRACT

The length of long bones is determined by column formation of proliferative chondrocytes and subsequent chondrocyte hypertrophy in the growth plate during bone development. Despite the importance of mechanical loading in long bone development, the mechanical conditions of the cells within the growth plate, such as the stress field, remain unclear owing to the difficulty in investigating spatiotemporal changes within dynamically growing tissues. In this study, the mechanisms of longitudinal bone growth were investigated from a mechanical perspective through column formation of proliferative chondrocytes within the growth plate before secondary ossification center formation using continuum-based particle models (CbPMs). A one-factor model, which simply describes essential aspects of a biological signaling cascade regulating cell activities within the growth plate, was developed and incorporated into CbPM. Subsequently, the developmental process and maintenance of the growth plate structure and resulting bone morphogenesis were simulated. Thus, stress anisotropy in the proliferative zone that affects bone elongation through chondrocyte column formation was identified and found to be promoted by chondrocyte hypertrophy. These results provide further insights into the mechanical regulation of multicellular dynamics during bone development.

1. Introduction

The longitudinal growth of long bones is regulated primarily by multicellular activities within the growth plate, which has a layered structure composed of proliferative, prehypertrophic, and hypertrophic zones at both ends of the primary spongiosa formed from the primary ossification center (POC) [1–5]. The growth plate is maintained during longitudinal bone growth before the secondary ossification center (SOC) formation at epiphysis, as well as after the SOC formation, by the sequential proliferation and hypertrophy of chondrocytes. In the proliferative zone of the growth plate, flattened proliferative cells form columns in the bone longitudinal axis through cell rearrangement after division [6–9]. Cell hypertrophy following proliferation in the columnar stack is a major cause of longitudinal bone growth [1]. Therefore, column formation of proliferative chondrocytes is an important regulator of bone length.

The cell differentiation and activities within the growth plate including column formation are regulated by many biological signaling molecules, such as Indian hedgehog (Ihh), parathyroid hormone-related protein (PTHrP), vascular endothelial growth factor (VEGF), and Wingless/Int (Wnt) [4,5,10–12]. Another important regulator of cell activity is mechanical loading from surrounding tissues, such as tendons, ligaments, and other bones [13–17]. Reportedly, mechanical stress induces the expression of Ihh, which promotes chondrocyte proliferation, and also affects column formation in the proliferative zone [10,13,17]. Despite the importance of mechanical loading in the regulation of cell

Abbreviations: 1D, One-dimensional; 3D, Three-dimensional; CbPM, Continuum-based particle model; DF, Differentiation factor; DPBS, Dulbecco's phosphate-buffered saline; EdU, 5-ethynyl-2′-deoxyuridine; FEM, Finite element method; Ihh, Indian hedgehog; PFA, Paraformaldehyde phosphate buffer solution; POC, Primary ossification center; PTHrP, Parathyroid hormone-related protein; SOC, Secondary ossification center.

* Corresponding author at: 53 Shogoin-Kawahara-cho, Sakyo-ku, Kyoto, 606-8507, Japan.
E-mail address: adachi@infront.kyoto-u.ac.jp (T. Adachi).

https://doi.org/10.1016/j.bone.2024.117055
Received 7 November 2023; Received in revised form 8 February 2024; Accepted 19 February 2024
Available online 25 February 2024

activities, measuring mechanical conditions such as the stress field within the growth plate in growing tissue remains difficult. Therefore, the mechanisms by which mechanical conditions spatiotemporally regulate cell activity during long bone development remain unclear.

Modeling and simulation are powerful strategies for estimating mechanical conditions and investigating the underlying mechanisms that cause cellular and tissue morphological changes. Recently, a novel multicellular simulation platform called continuum-based particle models (CbPMs) was developed [18]; this platform is capable of investigating tissue mechanical behaviors caused by multicellular dynamics in response to mechanical conditions. The calculation of tissue deformation based on continuum mechanics in CbPM can be effectively applied to simulate a growing-bone tissue composed of chondrocytes and the surrounding matrix, where the relative movement of cells in the tissue is often limited.

This study aimed to elucidate the mechanisms of longitudinal bone growth through column formation of proliferative chondrocytes within the growth plate before SOC formation from a mechanical perspective using CbPM. To investigate the mechanism by focusing on the mechanical behaviors of the tissue, a one-factor model, which describes essential aspects of the biological signaling cascade regulating cell activities within the growth plate, was developed and incorporated into CbPM. Three-dimensional (3D) multicellular modeling was performed to simulate the development and maintenance of the growth plate structure and the resulting bone morphogenesis. Thus, stress anisotropy in the proliferative zone, which affects the development of bone length and width through chondrocyte column formation, was identified and found to be promoted by chondrocyte hypertrophy.

2. Materials and methods

2.1. Hematoxylin and eosin staining

Metatarsals were extracted from ICR mice (Shimizu Laboratory Supplies Co., Ltd.) on embryonic days 14, 16, and 18 (E14, E16, and E18, respectively), fixed with 4 % paraformaldehyde phosphate buffer solution (PFA, Nacalai Tesque Inc.) for 2 h, and rinsed with Dulbecco's phosphate-buffered saline (DPBS). The sample was embedded for frozen block, cut with a thickness of 10 μm, and stained with hematoxylin and eosin via Kawamoto's film method 2020 using Cryofilm type 2C(9) and 4D(9) (Cryosection Preparation kit, SECTION-LAB Co. Ltd.) [19,20], a microtome blade (Feather, A35 type), and Leica CM1850 Cryostat (Leica Biosystems). The stained sections were observed under a BZ-X710 microscope (KEYENCE Co.) with a 40× objective lens (Nikon Co.). Mice experiments were approved by the Animal Experimentation Committee of Kyoto University (#Z19–2-4).

2.2. Fluorescence staining of DNA synthesizing cells

A 5-ethynyl-2′-deoxyuridine (EdU; Invitrogen) solution was prepared by dissolving the EdU in CO_2 independent medium (Gibco) containing 10 % fetal bovine serum (Gibco). Next, metatarsals extracted from E18 mice were cultured in 2 mM EdU solution at 37 °C for 24 h. Subsequently, the metatarsals were fixed with 4 % PFA for 2 h, rinsed with DPBS, and embedded in SCEM for frozen blocks. The cryosections were prepared with a thickness of 10 μm using the Cryofilm type 2C(9). After permeabilization with 0.5 % Triton® X-100 (MP Biomedicals) in 5 % BSA-DPBS (Nacalai Tesque Inc.) for 20 min and washing with DPBS, EdU detection was performed following the instruction stated in the Click-iT® EdU Alexa Fluor® 488 Imaging Kit (Invitrogen). Cell nuclei were stained with 4,6-diamidino-2-phenylindole dihydrochloride (DAPI; Nacalai Tesque Inc.). Fluorescence microscopy was performed using a FLUOVIEW FV3000 confocal laser scanning microscope (EVIDENT Co.).

2.3. One-factor model for cell differentiation

To investigate the mechanical behaviors of tissues during the development and maintenance of growth plates, a simple model of cell differentiation within the growth plate was constructed by considering a differentiation factor (DF) that expresses the integrated function of related biochemical signals (Figs. 1a and b). Assuming that DF diffuses within the tissue, the rate of DF concentration $C(\boldsymbol{x},t)$ at position $\boldsymbol{x}$ and time t depending on the production $S(\boldsymbol{x},t)$ of DF by the cells can be expressed as:

$$\frac{\partial C(\boldsymbol{x},t)}{\partial t} = D\nabla^2 C(\boldsymbol{x},t) + S(\boldsymbol{x},t) - kC(\boldsymbol{x},t), \tag{1}$$

where D and k are the diffusion coefficient and degradation rate constant of DF, respectively. The detailed diffusion analysis method is described in Section S1 in the supplementary file.

Given that Ihh promotes chondrocyte proliferation [10,13], resting chondrocytes, which comprise the entire chondrocyte condensation at an early stage of development, were modeled to differentiate into proliferative chondrocytes when the DF concentration $C(\boldsymbol{x},t)$ exceeds a threshold C_{prolif} (Figs. 1a and b). Furthermore, chondrocytes are also known to differentiate into prehypertrophic and hypertrophic states under the regulation of Ihh and PTHrP [21]. To express this differentiation process, the proliferative chondrocytes were modeled to differentiate into prehypertrophic chondrocytes when the DF concentration $C(\boldsymbol{x},t)$ exceeds the threshold C_{prehyp}. Additionally, Ihh is suggested to promote bone collar formation in the perichondrium region surrounding the bone tissue [1,10]. Therefore, bone collar was modeled to form when the DF concentration $C(\boldsymbol{x},t)$ exceeds the threshold C_{BC}.

In the hypertrophic zone, a previous study suggested that all hypertrophic cells turn over in approximately 1 day, which is common in various bones with different growth rates [22]. Thus, this study assumed that prehypertrophic and hypertrophic chondrocytes mature in the time durations T_{prehyp} and T_{hyp}, respectively (Figs. 1a and b). Herein, time t was measured from the time of onset of primary ossification center (POC) formation ($t = 0$). After prehypertrophic differentiation at time point $t = t_{\mathrm{diff}}$, the cell automatically differentiates into a hypertrophic state at $t = t_{\mathrm{diff}} + T_{\mathrm{prehyp}}$ and undergoes apoptosis to form primary spongiosa at $t = t_{\mathrm{diff}} + T_{\mathrm{prehyp}} + T_{\mathrm{hyp}}$.

Given that Ihh is produced by prehypertrophic and early hypertrophic chondrocytes [1,10,11,23], DF production by a cell was modeled to gradually increase as prehypertrophic chondrocytes mature and decrease after differentiation to a hypertrophic state by linearly changing the DF production $S(\boldsymbol{x},t)$ at position $\boldsymbol{x}$ in the domain of the cell with time, as illustrated in Fig. 1b-2, as follows

$$S(\boldsymbol{x},t) = \begin{cases} S_{\max}\dfrac{t - t_{\mathrm{diff}}}{T_{\mathrm{prehyp}}} & \left(t_{\mathrm{diff}} \le t < t_{\mathrm{diff}} + T_{\mathrm{prehyp}}\right) \\ S_{\max}\left(1 - \dfrac{t - t_{\mathrm{diff}} - T_{\mathrm{prehyp}}}{0.5T_{\mathrm{hyp}}}\right) & \left(t_{\mathrm{diff}} + T_{\mathrm{prehyp}} \le t < t_{\mathrm{diff}} + T_{\mathrm{prehyp}} + 0.5T_{\mathrm{hyp}}\right) \\ 0\,(\mathrm{else}) & \end{cases} \tag{2}$$

where $S_{\max}$ is the maximum DF production.

Previous studies have measured the diffusion coefficients of various bioactive molecules using techniques such as fluorescence recovery after photobleaching [24,25]. In a previous study simulating the reaction-diffusion system in bone development, values between 8.2×10^{-12} and 1.1×10^{-10} m^2/s were used as the diffusion coefficient of Ihh and PTHrP [26]. In the present study, the diffusion coefficient of DF was set as $D = 1.0 \times 10^{-12}$ m^2/s, which is within the same range as that in previous studies. The degradation rate constant of DF, k, was arbitrarily set to $k = 0.005/s$. The threshold of DF concentration for proliferative differentiation C_{prolif} and that for prehypertrophic differentiation C_{prehyp} were determined as $C_{\mathrm{prolif}} = 0.5$ pM/μm^3 and $C_{\mathrm{prehyp}} = 30.0$ pM/μm^3,

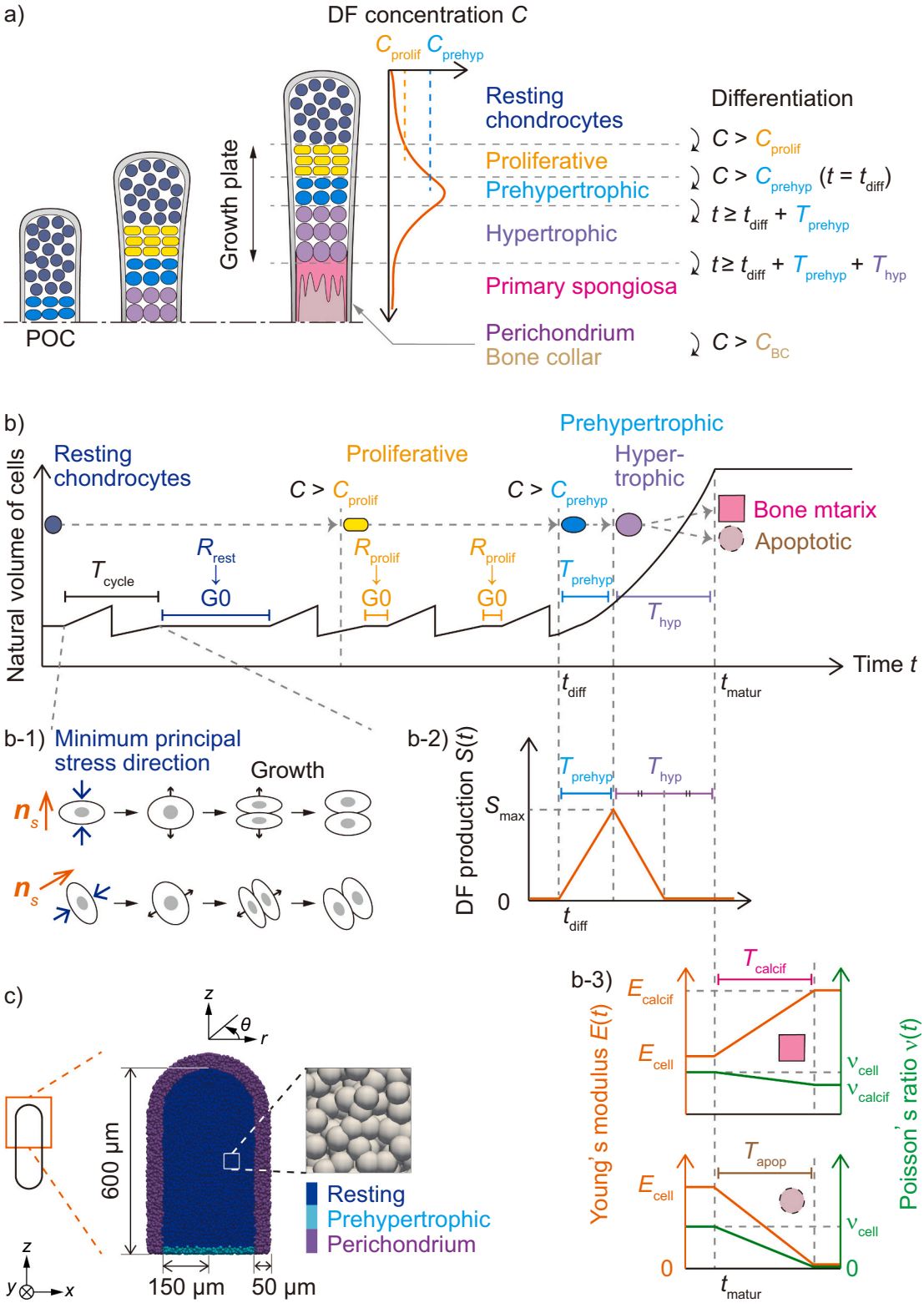

Fig. 1. One-factor model and cell dynamics model. a) Development of a growth plate composed of proliferative, prehypertrophic and hypertrophic zones after the onset of POC formation at the center of the bone, and regulation of cell differentiation by DF; here, a half of a long bone is depicted. b) Time-dependent change in natural volume of cells due to proliferation and hypertrophy. b-1) Modeling of cell proliferation. Cells grow and divide in the direction of division $\boldsymbol{n}_s$, which was assumed to be the most compressive direction of the cell, that is, the minimal principal stress direction. b-2) Production of DF by prehypertrophic and hypertrophic chondrocytes. b-3) Change in Young's modulus and Poisson's ratio expressing calcification and apoptosis. c) Initial condition of 3D simulation. Each sphere indicates a material point, assumed to represent a cell and surrounding chondrocyte matrix.

respectively, through one-dimensional (1D) simulation of the growth plate described in Sections S2 and S3 to reproduce reasonable lengths of both the proliferative and hypertrophic zones [27]. The threshold of DF concentration for bone collar formation C_{BC} was determined as $C_{BC} = 10.0\ \mathrm{pM}/\mu\mathrm{m}^3$ through 3D multicellular simulation based on the cell dynamics model described later in Section 2.4, such that sufficiently calcified bone collar can be observed near the hypertrophic zone, as shown in Section S4 [1]. The time duration of chondrocyte hypertrophy T_{hyp} was set to 1 day referring to [22], and the time duration of prehypertrophy T_{prehyp} was arbitrarily set to 0.5 days as a comparative length with T_{hyp}. The value of S_{max} was arbitrarily set to $S_{max} = 1.0\ \mathrm{pM}/\mu\mathrm{m}^3/\mathrm{s}$.

2.4. Cell dynamics model in CbPM

To simulate the mechanical behaviors of growing bone tissue derived from multicellular dynamics within the growth plate, the one-factor model described in Section 2.3 was incorporated into the CbPM [18]. In CbPM, material points, each of which can be assumed to represent an individual cell and the surrounding matrix, are used to discretize the entire bone tissue. Cell growth was modeled based on the theory of finite growth [28,29], where the deformation gradient at material point p, $\boldsymbol{F}_p$, is multiplicatively decomposed as:

$$\boldsymbol{F}_p = \boldsymbol{F}_p^e \boldsymbol{F}_p^g \tag{3}$$

where $\boldsymbol{F}_p^e$ and $\boldsymbol{F}_p^g$ represent the elastic and growth components of the deformation gradient, respectively. The developing bone tissue was assumed to obey the compressible neoHookean model [30], in which strain energy density Ψ in reference configuration is expressed as:

$$\Psi = J^g \left(\frac{\lambda}{8} ln^2 I_3 + \frac{\mu}{2} (I_1 - 3 - ln I_3) \right) \tag{4}$$

where J^g is Jacobian of $\boldsymbol{F}_p^g$; λ and μ are Lame's constants; and I_1 and I_3 are the first and third invariants of the elastic part of the right Cauchy–Green tensor, $\boldsymbol{C}_p^e = \boldsymbol{F}_p^{eT} \boldsymbol{F}_p^e$, respectively. The Lame's constants can be expressed using Young's modulus, E, and Poisson's ratio, ν, as $\lambda = \frac{E\nu}{(1+\nu)(1-2\nu)}$ and $\mu = \frac{E}{2(1+\nu)}$.

2.4.1. Cell proliferation

Cell proliferations of resting and proliferative chondrocytes were modeled by combining the unidirectional growth of a material point in the direction of division $\boldsymbol{n}_s$ for time duration T_{cycle} of G1, S, G2, and M phases and division of the material point in the M phase (Fig. 1b-1) [18]. Unidirectional growth was expressed by setting the growth part of the deformation gradient $\boldsymbol{F}_p^g$ and the growth stretch θ as:

$$\boldsymbol{F}_p^g = (\boldsymbol{I} + (\theta - 1)\boldsymbol{n}_s \otimes \boldsymbol{n}_s)\boldsymbol{F}_{p\_pre}^g \tag{5}$$

$$\theta = 1 + \frac{t - t_{pre}}{T_{cycle}}, \frac{D\theta}{Dt} = 1 \Big/ T_{cycle} \tag{6}$$

where $\boldsymbol{I}$ is the second-order identity tensor and $\boldsymbol{F}_{p\_pre}^g$ is the growth part of the deformation gradient before the onset of the S phase at time point $t = t_{pre}$. The growth stretch θ increased linearly from 1.0 to 2.0 for T_{cycle}, essentially expressing the growth at a constant rate. After a cell cycle, the cells remain in the quiescent G0 phase until the next cell cycle begins (Fig. 1b). Considering that the onset of the cell cycle occurs continuously and independently at a constant average rate, herein, the duration of the G0 phase was assumed to follow an exponential distribution, with the rate parameter R_{rest} for resting chondrocytes and R_{prolif} for proliferative chondrocytes [18].

Proliferative cells in the growth plate are known to divide with the division plane bisecting the long axis of the cell. After division, the two daughter cells rearrange into columns along the bone longitudinal axis [6–9]. For cell rearrangement, cell-cell adhesion between the two daughter cells due to enriched cadherins is necessary [6,9]. Cell morphology under cell-cell adhesion conditions can be determined by an energy function combining membrane elasticity and adhesion [31]. According to the energy function, tighter adhesion between two cells leads to expansion of their interface area [31–34]. Considering mechanical confinement by the chondrocyte matrix surrounding the two daughter cells, the two cells can be assumed to align with the shortest axis of the parent cell morphology to realize the largest interface area corresponding to a low-energy state. Based on these findings [6,9,31–34], direction $\boldsymbol{n}_s$ was assumed to be the most compressive direction of the cell, that is, the minimal principal stress direction, to describe the cell alignment after rearrangement (Fig. 1b-1). Therefore, with the vertical direction being the minimal principal stress direction, the cell will grow only in the vertical direction, and there will be no growth in the transverse direction (Fig. 1b-1 top). It should be noted that the alignment direction of cells after division, which is also the most compressive direction, is not necessarily the macroscopic bone longitudinal direction, because there is no other assumption in our model to align the cells or to compress them in an arbitrary direction.

The total cell cycle time in the proliferative zone, which depends on the bone growth rate, has been estimated based on bromodeoxyuridine pulse labeling [35]. Because the growth rate of the third metatarsal is approximately 300 μm/day [27], the total duration of a cell cycle, including the G0 phase, can be estimated to be approximately 30–34 h [35]. Based on these studies, herein, $T_{cycle} = 1.0$ day and a rate parameter of exponential distribution for proliferative chondrocytes of $R_{prolif} = 5.0/\mathrm{day}$ were adopted; the resulting average length of the G0 phase was $\frac{1}{R_{prolif}} = 0.2$ days. Furthermore, the frequency of cell division is lower in the resting zone than in the proliferative zone (Fig. 1b). Thus, the rate parameter for resting chondrocytes was estimated as $R_{rest} = 1.0/\mathrm{day}$ (the resulting average length of the G0 phase was $^1/_{R_{rest}} = 1.0$ day) based on the comparison between the simulation and EdU staining of the mouse third metatarsal, as described later in Section 3.1.

2.4.2. Cell prehypertrophy

Cell prehypertrophy can be observed as the enlargement of cells in the columns formed owing to cell proliferation. To reproduce these cell dynamics, prehypertrophic chondrocytes were modeled to complete the ongoing cell cycle by faster growth compared with proliferative chondrocytes, and isotropic growth was initiated in the same way as for hypertrophic chondrocytes described in Section 2.4.3 (Fig. 1b). The faster growth to complete the cell cycle was expressed by a doubled increase rate of the growth stretch in Eq. 6 as:

$$\frac{D\theta}{Dt} = 2 \Big/ T_{cycle} \tag{7}$$

2.4.3. Cell hypertrophy

Considering that hypertrophic chondrocytes grow due to osmotic pressure [36], hypertrophic and prehypertrophic chondrocytes were modeled to grow isotropically after the completion of the cell cycle (Fig. 1b) by setting the growth part of the deformation gradient $\boldsymbol{F}_p^g$ and growth stretch θ as:

$$\boldsymbol{F}_p^g = \theta \boldsymbol{F}_{p\_pre}^g \tag{8}$$

$$\theta = \sqrt[3]{G}^{t - t_{pre}} \tag{9}$$

where $\boldsymbol{F}_{p\_pre}^g$ is the growth part of the deformation gradient before the onset of isotropic growth at time $t = t_{pre}$, G is the growth constant. This formula indicates cell growth of G times in volume in 1 day.

The cell number density in the hypertrophic zone has been reported to be, on average, one-fifth of that in the proliferative zone [37]. To

consider the difference in the cell number density, the prehypertrophic and hypertrophic cells were assumed to grow to three times in volume in 1 day by setting $G = 3.0$; consequently, they were estimated to grow approximately five times in volume in 1.5 days ($= T_{\mathrm{prehyp}} + T_{\mathrm{hyp}}$).

2.4.4. Calcification and apoptosis

After the maturation of hypertrophic chondrocytes at time $t = t_{\mathrm{matur}} = t_{\mathrm{diff}} + T_{\mathrm{prehyp}} + T_{\mathrm{hyp}}$, hypertrophic chondrocytes undergo apoptosis and provide space for the formation of irregular spicules called primary spongiosa (Fig. 1a) [1,36]. To model the formation of this structure, half of the mature hypertrophic chondrocytes were assumed to be gradually replaced by a calcified bone matrix, and the other half underwent apoptosis to create empty space (Fig. 1b). Whether the mature hypertrophic chondrocytes became calcified or empty region was determined randomly, considering that the primary spongiosa has no distinct structural features.

In the process of replacement from the hypertrophic chondrocytes to calcified bone matrix, the Young's modulus $E(t)$ and Poisson's ratio $\nu(t)$ of the material point were assumed to change linearly with time, from the values of cells to that of bone matrix for a time duration T_{calcif}, as illustrated in Fig. 1b-3 (top), as follows.

$$E(t) = E_{\mathrm{cell}}\frac{\left(t_{\mathrm{matur}} + T_{\mathrm{calcif}} - t\right)}{T_{\mathrm{calcif}}} + E_{\mathrm{calcif}}\frac{\left(t - t_{\mathrm{matur}}\right)}{T_{\mathrm{calcif}}} \quad \left(t_{\mathrm{matur}} \le t < t_{\mathrm{matur}} + T_{\mathrm{calcif}}\right) \tag{10}$$

$$\nu(t) = \nu_{\mathrm{cell}}\frac{\left(t_{\mathrm{matur}} + T_{\mathrm{calcif}} - t\right)}{T_{\mathrm{calcif}}} + \nu_{\mathrm{calcif}}\frac{\left(t - t_{\mathrm{matur}}\right)}{T_{\mathrm{calcif}}} \quad \left(t_{\mathrm{matur}} \le t < t_{\mathrm{matur}} + T_{\mathrm{calcif}}\right) \tag{11}$$

where E_{cell} and ν_{cell} are Young's modulus and Poisson's ratio of chondrocytes, respectively; and E_{calcif} and ν_{calcif} are Young's modulus and Poisson's ratio of calcified bone matrix, respectively. Through this process, the residual stress was assumed to be eliminated by updating the growth part of the deformation gradient $\boldsymbol{F}_{\mathrm{p}}^{\mathrm{g}}$, as follows.

$$\boldsymbol{F}_{\mathrm{p}}^{\mathrm{g}} = \boldsymbol{F}_{\mathrm{p}} \tag{12}$$

which indicates the formation of the fresh matrix at the current configuration.

For the process of apoptosis of the hypertrophic chondrocytes, the Young's modulus $E(t)$ and Poisson's ratio $\nu(t)$ were modeled to decrease linearly with time to zero for a time duration T_{apop}, as illustrated in Fig. 1b-3 (bottom), as follows.

$$E(t) = E_{\mathrm{cell}}\frac{\left(t_{\mathrm{matur}} + T_{\mathrm{apop}} - t\right)}{T_{\mathrm{apop}}} \quad \left(t_{\mathrm{matur}} \le t < t_{\mathrm{matur}} + T_{\mathrm{apop}}\right) \tag{13}$$

$$\nu(t) = \nu_{\mathrm{cell}}\frac{\left(t_{\mathrm{matur}} + T_{\mathrm{apop}} - t\right)}{T_{\mathrm{apop}}} \quad \left(t_{\mathrm{matur}} \le t < t_{\mathrm{matur}} + T_{\mathrm{apop}}\right), \tag{14}$$

which indicates the gradual degradation and elimination of the existing structure.

The perichondrium surrounding bone tissue was modeled as an elastic tissue that has mechanical properties of chondrocytes and can stretch passively but does not actively grow or proliferate. The formation of bone collar, which is composed of bone matrix, in the region of perichondrium was modeled in the same way as calcification of hypertrophic chondrocytes, by varying Young's modulus $E(t)$ and Poisson's ratio $\nu(t)$ of the material point for a time duration T_{calcif}, as follows.

$$E(t) = E_{\mathrm{cell}}\frac{\left(t_{\mathrm{BC}} + T_{\mathrm{calcif}} - t\right)}{T_{\mathrm{calcif}}} + E_{\mathrm{calcif}}\frac{\left(t - t_{\mathrm{BC}}\right)}{T_{\mathrm{calcif}}} \quad \left(t_{\mathrm{BC}} \le t < t_{\mathrm{BC}} + T_{\mathrm{calcif}}\right) \tag{15}$$

$$\nu(t) = \nu_{\mathrm{cell}}\frac{\left(t_{\mathrm{BC}} + T_{\mathrm{calcif}} - t\right)}{T_{\mathrm{calcif}}} + \nu_{\mathrm{calcif}}\frac{\left(t - t_{\mathrm{BC}}\right)}{T_{\mathrm{calcif}}} \quad \left(t_{\mathrm{BC}} \le t < t_{\mathrm{BC}} + T_{\mathrm{calcif}}\right) \tag{16}$$

where t_{BC} is the time at which bone collar formation begins. Through this process, the residual stress was eliminated according to Eq. 12.

The material properties of cells E_{cell} and ν_{cell} were set to $E_{\mathrm{cell}} = 1.0$ kPa and $\nu_{\mathrm{cell}} = 0.4$, respectively, by considering the order of the measured values for chondrocytes [38,39]. The Young's modulus of the immature bone matrix E_{calcif} was set to $E_{\mathrm{calcif}} = 1.0$ MPa, which is sufficiently large relative to E_{cell}. The Poisson's ratio of the bone matrix ν_{calcif} was set as $\nu_{\mathrm{calcif}} = 0.3$, by considering the order of the measured values for human femur [40]. The duration of calcification T_{calcif} and apoptosis T_{apop} were set to $T_{\mathrm{calcif}} = 1.0$ day and $T_{\mathrm{apop}} = 1.0$ day as the same order as the duration of the cell cycle and cell hypertrophy. All parameters used in the models are listed in Table S1.

2.4.5. Initial conditions

The distal half of a mouse third metatarsal was modeled for analysis because of its simple and axisymmetric shape. Initial chondrocyte condensation was modeled as a capsule combining a cylinder with a radius of 150 μm and half-length of 450 μm, and two hemispheres with a radius of 150 μm (Fig. 1c left) by mimicking the shape of the E14 mouse metatarsal. This entirely 3D model was composed of resting chondrocytes surrounded by a perichondrium with a thickness of 50 μm (Fig. 1c center). The position $\boldsymbol{x}$ was determined based on the center of the capsule, and the z-axis was set as the longitudinal axis of the cylinder. The x- and y-axes were arbitrarily set perpendicular to the z-axis. The radial (r) and circumferential (θ) axes were set in the plane perpendicular to the z-axis. By considering mirror symmetry on the $x = 0$, $y = 0$, and $z = 0$ planes, one-eighth of the whole tissue, that is, one-fourth of the distal half of the chondrocyte condensation was modeled, and slip boundary conditions were applied for the $x = 0$, $y = 0$, and $z = 0$ planes of this entirely 3D model. To avoid any undesirable effects in data analyses due to the boundaries, data for any graphs regarding proliferative chondrocytes were collected from the off-axis region ($x \ge 10$, $y \ge 10$, and $z \ge 10$ (μm)). Additionally, data from the outer region ($r > 150$ (μm)) were not included, because the peripheral region of the bone has different mechanical conditions owing to the effects of the perichondrium and bone collar. The initial volume of the material points was assumed to follow a normal distribution of $N\left(V_{\mathrm{ave}}, {V_{\mathrm{dev}}}^2\right)$, based on its average V_{ave} and standard deviation V_{dev}, to consider the individual differences in cells. The material points were distributed randomly with a uniform density within the 3D tissue in the initial condition (Fig. 1c right).

The average volume of material points V_{ave} was set as $V_{\mathrm{ave}} = 10^3\ \mu\mathrm{m}^3$, based on the order of the inverse of cell density in the resting zone [37]. The standard deviation of the volume of material points V_{dev} was set as $V_{\mathrm{dev}} = 10^2\ \mu\mathrm{m}^3$ such that the probability distribution of the volume of material points was reasonable (approximately 95 % of the material points have volume between 800 and 1200 $\mu\mathrm{m}^3$). Furthermore, all material points were confirmed to have a volume >500 $\mu\mathrm{m}^3$, and be smaller than 1500 $\mu\mathrm{m}^3$ in the initial state. The onset of POC formation was modeled by prehypertrophic differentiation near the $z = 0$ plane in the initial chondrocyte condensation [1] (Fig. 1c center). The initial DF concentration $C(\boldsymbol{x}, 0)$ was set to 0 as no prehypertrophic or hypertrophic chondrocytes produced DF before the onset of POC formation.

3. Results

3.1. 3D multicellular simulation of growth plate development and maintenance

To investigate the mechanism of longitudinal bone growth from a mechanical perspective, a 3D multicellular simulation of the growth plate development was conducted (Fig. 2a and Video 1). Initial chondrocyte condensation (Day 0 in Fig. 2a) was confirmed to mimic the E14 mouse metatarsal (E14 in Fig. 2b). After the onset of POC formation at Day 0, a growth plate composed of proliferative, prehypertrophic, and

hypertrophic zones developed within 2 days (Day 2 in Fig. 2a). During the following 2 days of simulation (from Day 2 to Day 4 in Fig. 2a), the growth plate structure was maintained and the entire bone tissue elongated because of differentiation, proliferation, and hypertrophy of the composing cells. The simulated growth plate development and maintenance were phenomenologically consistent with those observed in the HE staining of E16 and E18 mouse metatarsals (Fig. 2b), where the proliferative (P), prehypertrophic (PH), and hypertrophic (H) zones composing the growth plate are indicated. Proliferative (P) chondrocytes have a flattened cell shape, whereas prehypertrophic (PH) and hypertrophic (H) chondrocytes can be distinguished by their gradually increasing cell volume.

The proliferative zone in the growth plate and the region of resting chondrocytes can be distinguished by differences in the frequency of division. EdU staining was performed to label newly synthesized DNA in the third metatarsal of E18 mice (Fig. 2c), and it revealed that the percentage of EdU-positive cells in the proliferative zone was approximately two times larger than the percentage of resting chondrocytes (Fig. 2d). Furthermore, the frequency of division of resting chondrocytes can be regulated in the simulation by varying the rate parameter of proliferation for resting chondrocytes R_{rest}. To confirm that the simulation based on CbPM can express the physiological differences in the frequency of division depending on the cell type, the percentage of cells in the S phase (within 6 h after the onset of the S phase) on Day 4 was calculated (Fig. 2e). Subsequently, under the rate parameter $R_{\mathrm{rest}} = 1.0/\mathrm{day}$, the percentage of cells in the S phase in the proliferative zone was approximately two times larger than the percentage of resting chondrocytes (Fig. 2f); this trend is similar to that observed with EdU staining (Fig. 2d). Thus, the development and maintenance of the growth plate with reasonable differences in the frequency of division depending on the cell types were simulated based on our models.

3.2. Stress anisotropy in the proliferative zone promoting column formation

Within the growth plate, column formation of proliferative chondrocytes along the bone longitudinal axis is an important regulator of longitudinal bone growth. Chondrocyte columns were observed in the HE staining of the E16 mouse metatarsals (Fig. 3a). In the simulation (Fig. 3b), the direction $\boldsymbol{n}_{\mathrm{s}}$ of cell alignment after rearrangement was confirmed to be uniformly close to the z-axis, as shown by the histogram of the direction $\boldsymbol{n}_{\mathrm{s}}$ in Fig. 3c, indicating column formation along the z-axis.

To investigate the mechanism of column formation, the stress field (Fig. 3d), which determines the direction $\boldsymbol{n}_{\mathrm{s}}$ (Fig. 3e) of cell alignment after rearrangement in our models, was analyzed. Normal stresses, σ_r, σ_θ, σ_z, in radial (r), circumferential (θ), and bone longitudinal (z) directions, respectively, were calculated and are indicated in Fig. 3d; the stress condition in the proliferative zone was qualitatively different from that in the hypertrophic zone. Stress in all three directions were negative in

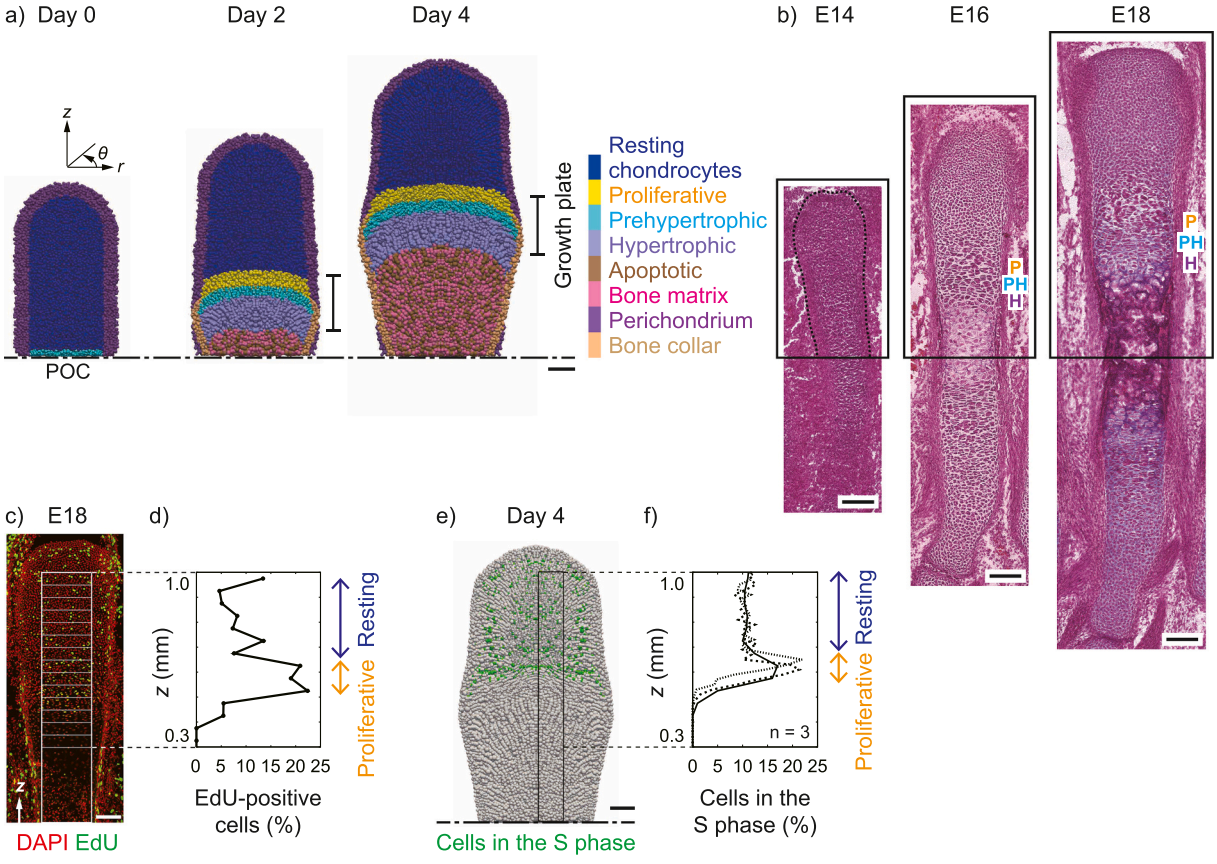

Fig. 2. Growth plate development and maintenance in the 3D simulation of mouse third metatarsals. a) Development and maintenance of the growth plate in 3D simulation; here, the views of the $y = 50$ μm plane of half of the tissue at 0, 2, and 4 days after the onset of POC formation (Days 0, 2, and 4) are shown. b) HE staining of third metatarsal of E14, E16, and E18 mice; here, P: proliferative zone, PH: prehypertrophic zone, and H: hypertrophic zone. c) Fluorescent images of an E18 mouse third metatarsal; here, red: DAPI (DNA), whereas green: EdU (newly synthesized DNA). d) Percentages of EdU-positive cells from the area, as indicated by the white frame (width, 200 μm) in the fluorescent image (c) $(0.3 < z < 1.0\ (\mathrm{mm}))$. e) Cells in the S phase (green) and other cells composing the tissue at Day 4 in the simulation; here, the view of the $y = 10$ μm plane of half of the tissue is shown. f) Percentages of cells in the S phase from the area, as indicated by the black frame (width, 100 μm; thickness, 10 μm) in the cross-section (e) $(0.3 < z < 1.0\ (\mathrm{mm}))$, which corresponds to the analysis area in the fluorescent image of the 10 μm section of the mouse metatarsal in (c) considering the symmetry of the simulation. Data from the three simulation results based on different initial random configurations of cells were used. Scale bars: 100 μm. (For interpretation of the references to color in this figure legend, the reader is referred to the web version of this article.)

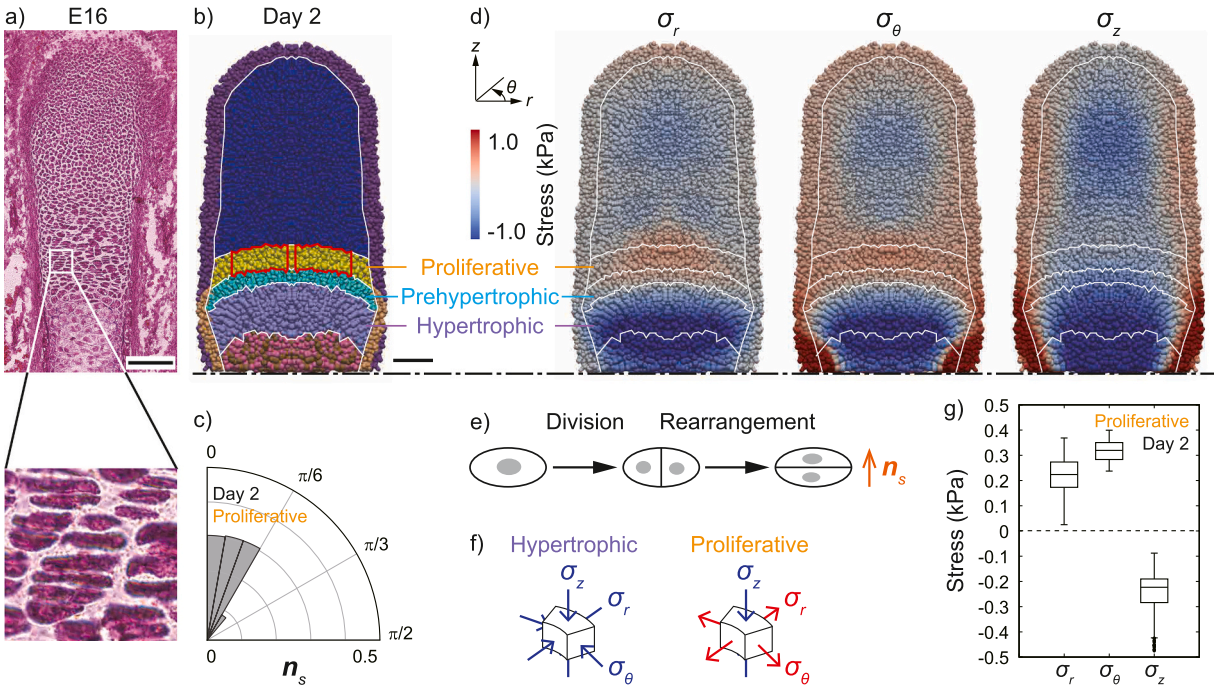

Fig. 3. Chondrocyte columns and stress field within the growth plate. a) HE staining of the third metatarsal of an E16 mouse. b) Growth plate structure in 3D simulation at Day 2; here, the view of the $y = 50$ μm plane of half of the tissue is shown. Data for any graphs regarding proliferative chondrocytes were collected from the inner and off-axis region ($r \leq 150, x \geq 10, y \geq 10$, and $z \geq 10$ (μm)), as indicated by the red frame. c) Histogram of the division direction $\boldsymbol{n}_s$ of proliferative cells in the region indicated by the red frame in (b) at Day 2, measured from the z-axis; here, cell number is divided by the solid angle of the corresponding direction of division and normalized. d) Distribution of stress in radial (σ_r), circumferential (σ_θ), and bone longitudinal (σ_z) directions at Day 2. e) Diagram of cell division and following rearrangement to align in the most compressive direction of the parent cell. f) Stress in the hypertrophic and proliferative zones. g) Stress in radial (σ_r), circumferential (σ_θ), and bone longitudinal (σ_z) directions of proliferative cells at Day 2. Scale bars: 100 μm. (For interpretation of the references to color in this figure legend, the reader is referred to the web version of this article.)

the hypertrophic zone, thus indicating volumetric compression (Figs. 3d and f). By contrast, in the proliferative zone, the stress in the bone longitudinal direction (σ_z) was negative (compressive), whereas the stress in radial (σ_r) and circumferential (σ_θ) directions were positive (tensile) (Fig. 3d), thus indicating in-plane tension in the disc-like proliferative zone in the growth plate (Fig. 3f). The positive stress in r- and θ-directions and the negative stress in z-direction in the proliferative zone are also confirmed in Fig. 3g. These results suggest that chondrocyte column formation along the bone longitudinal axis (z) was due to stress anisotropy in the proliferative zone determined by the in-plane tension in the transverse plane and compression in the z-direction.

3.3. Development of the bone shape is affected by chondrocyte column formation depending on the stress anisotropy

To assess the effect of the relationship between the stress field and column formation on long bone development, the disruption of cell rearrangement after division, which is observed under the reduction of cadherin binding [6] or deletion of β1 integrin gene expression [8], was considered. By setting the direction of cell division $\boldsymbol{n}_s$ as the most extensive direction of the parent cell, that is, the maximum principal stress direction (Fig. 4a), a situation without cell rearrangement was simulated (Fig. 4b; hereinafter referred to as No-rearrangement simulation). As expected, the tendency of the division direction $\boldsymbol{n}_s$ to be close to the z-axis disappeared (Fig. 4c), thus indicating the failure of column formation along the bone longitudinal axis. The failure of the column formation was due to compressive stress in the bone longitudinal direction (σ_z), and tensile stress in radial (σ_r) and circumferential (σ_θ) directions (Fig. 4d).

Disruption of cell rearrangement also affected the development of bone shape (Fig. 4b). As shown in Fig. 4e, the half-length of the tissue, including the perichondrium and bone collar, grew slower in the No-rearrangement simulation than in the simulation with normal cell rearrangement (Figs. 2 and 3; hereinafter referred to as Normal simulation) during the development and maintenance of the growth plate (Days 0–4). The width of the entire tissue grew faster in the No-rearrangement simulation (Fig. 4f). The shorter and broader bone shape was consistent with the observation of bones with deletion of β1 integrin gene expression [8]. Thus, our simulation based on CbPM enabled the analysis of the development of bone shape caused by individual cell activities in the growth plate, and revealed the importance of the relationship between the stress field and column formation in bone growth.

3.4. Chondrocyte hypertrophy promotes stress anisotropy in the proliferative zone

To investigate the cause of the anisotropic stress field in the proliferative zone affecting the development of bone shape through column formation, chondrocyte hypertrophy in the prehypertrophic and hypertrophic zones was considered as the major cell activity in the vicinity of the proliferative zone. To observe the effect of chondrocyte hypertrophy on the stress field, growth plate development without cell growth of prehypertrophic and hypertrophic chondrocytes after the completion of the cell cycle was simulated by setting growth constant as $G = 1.0$ (Figs. 5a and b; hereinafter referred to as No-growth simulation).

In this case, stress in the radial (σ_r) and circumferential (σ_θ) directions in most parts of the proliferative zone, as well as that in the bone longitudinal direction (σ_z), was smaller than zero (compressive) (Fig. 5c), thus indicating that the in-plane tension observed in Normal simulation (Figs. 3d, f and g) disappeared. The analysis of stress in the proliferative zone in simulations with different values of growth constant G (Fig. 5a) revealed that stress in the radial (σ_r) and circumferential (σ_θ) directions increased monotonically with change in the growth

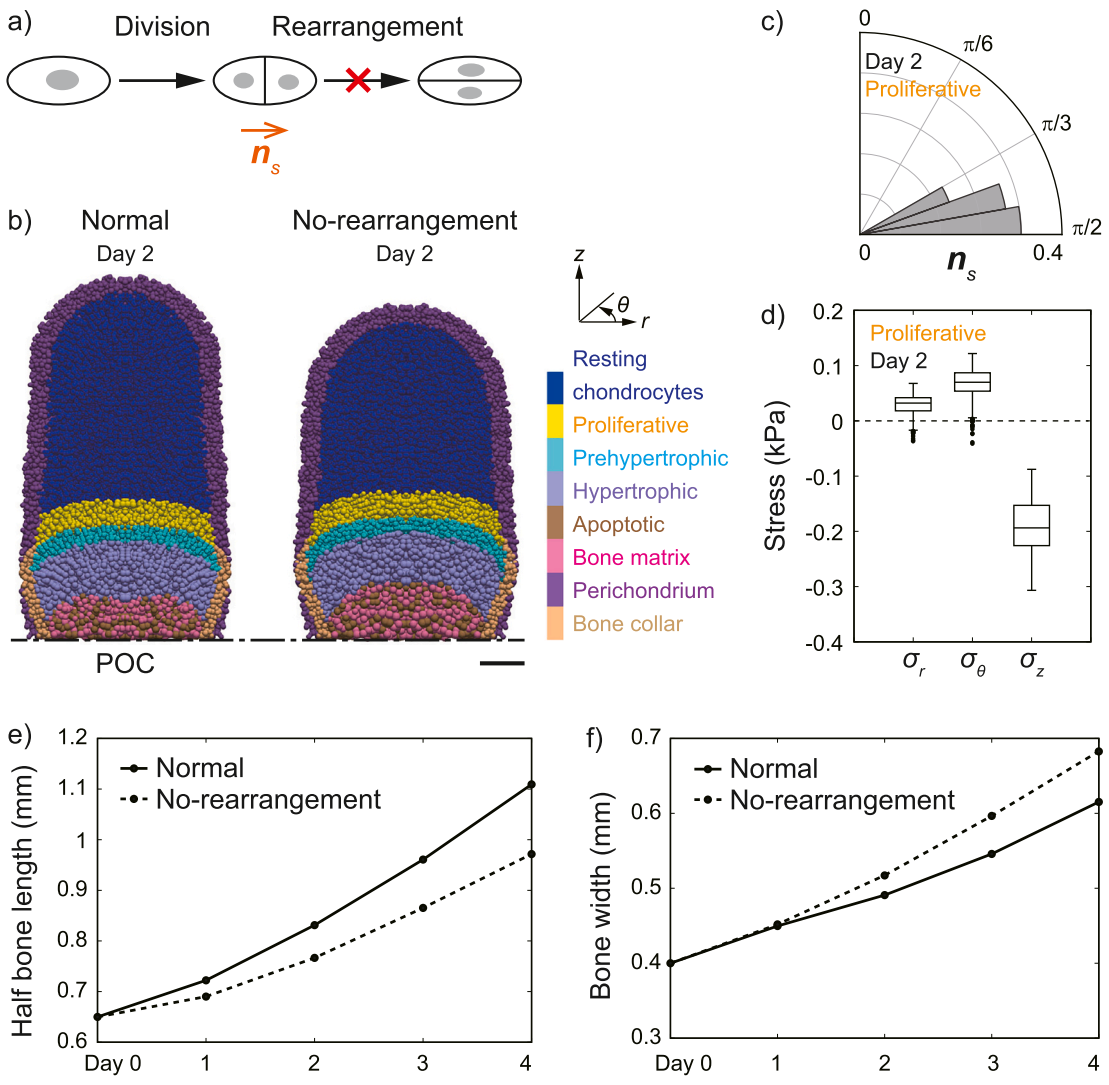

Fig. 4. Effect of column formation on the development of bone shape. a) Diagram indicating the disruption of cell rearrangement after division. b) Growth plate structure in the simulations with (Normal) and without cell rearrangement (No-rearrangement) at Day 2; here, the view of the $y = 50$ μm plane of half of the tissues is shown. c) Histogram of the division direction $\boldsymbol{n}_s$ in the proliferative zone at Day 2 in the No-rearrangement simulation, measured from the z-axis. d) Stress in radial (σ_r), circumferential (σ_θ), and bone longitudinal (σ_z) directions of proliferative cells at Day 2 in the No-rearrangement simulation. e) Change in the half-length of tissues in the Normal and No-rearrangement simulations. f) Change in the width of tissues in the Normal and No-rearrangement simulations. Scale bar: 100 μm.

constant G (Fig. 5d). Consequently, the stress anisotropy, which can be evaluated by the difference between maximum ($\sigma_{\max}$) and minimum ($\sigma_{\min}$) principal stresses, was smaller in the No-growth simulation ($G = 1.0$) than in the Normal simulation ($G = 3.0$) (Fig. 5e). The representative deformation states of the cells are indicated by yellow ellipses in Fig. 5e. This result suggests that cells in the Normal condition can rearrange into columns more easily than the cells in the No-growth condition because of the flattened shapes of the parent cells owing strongly to stress anisotropy. We also confirmed that all parameters that were arbitrarily set or fitted to the simulation (i.e., were not based on experimental measurements) had little effect on stress anisotropy in the proliferative zone (Section S5 in the supplementary file). Therefore, stress anisotropy in the proliferative zone determined by in-plane tension, which affects bone development through column formation, was shown to be promoted by chondrocyte hypertrophy.

4. Discussion

To elucidate the mechanisms of longitudinal bone growth from a mechanical perspective, herein, the developmental process and maintenance of the growth plate were simulated by developing a one-factor model for cell differentiation and incorporating it into CbPM. As a result of the investigation, stress anisotropy in the proliferative zone, which affects the development of bone length and width through chondrocyte column formation, was identified and found to be promoted by chondrocyte hypertrophy (Fig. 6a).

Finite element method (FEM) effectively simulates the tissue-level deformation of developing bones [26,41,42]. However, the analysis based on FEM does not consider individual cell activities, such as division in different directions at different timings. In this study, CbPM, in which the tissue is discretized by material points that represent a cell and the surrounding matrix, was applied. Based on CbPM, although cell morphology and cell-cell connectivity at the single-cell level cannot be obtained, individual cell activities such as division and hypertrophy can be explicitly expressed and incorporated into deformation analysis at the tissue level. This multiscale strategy using CbPM enabled stress analysis within the growth plate (Figs. 3d and 5c) and the prediction of changes in bone length and width (Figs. 4e and f) caused by individual cell activities, depending on the mechanical conditions (Figs. 3e and 4a). This approach can contribute to connecting single-cell- and tissue-level

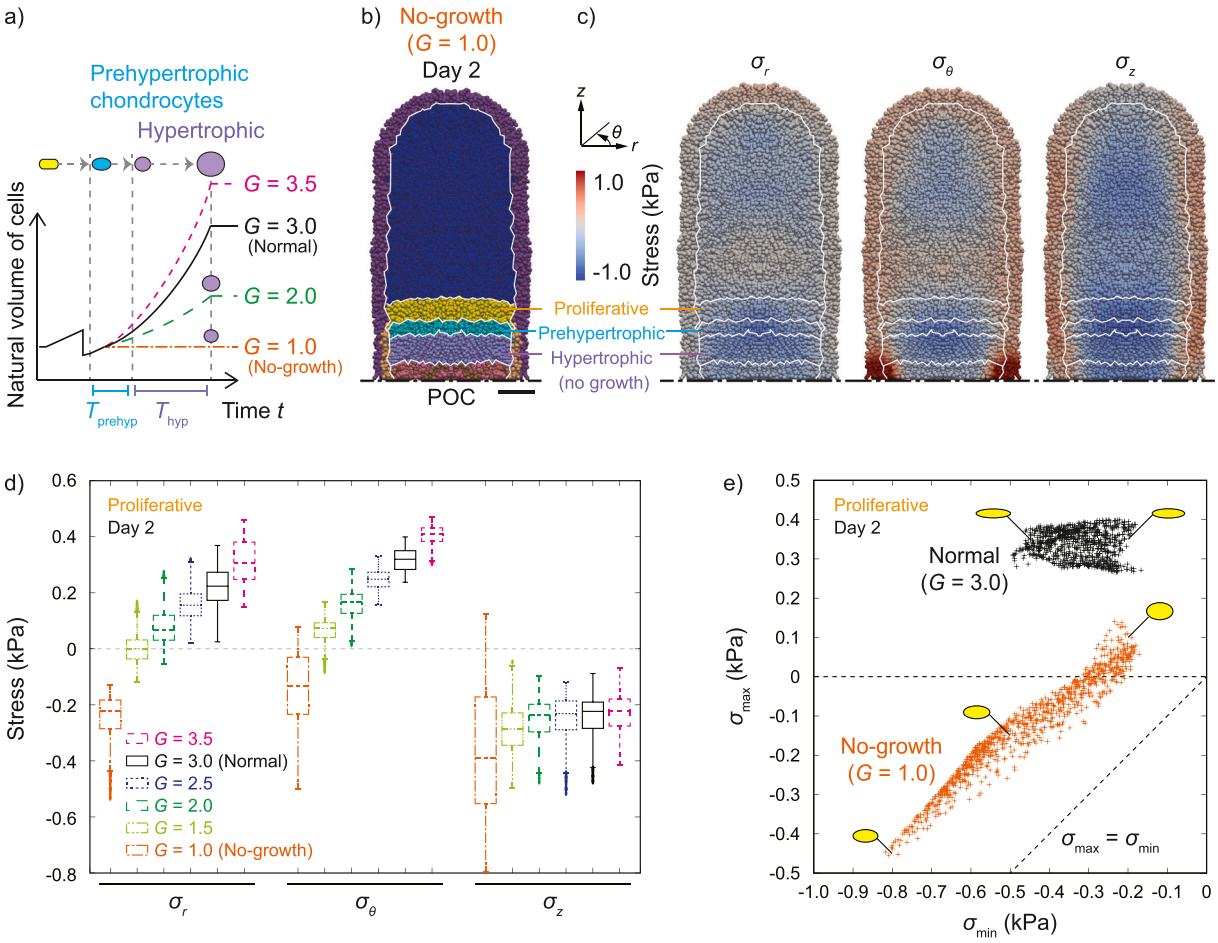

Fig. 5. Effect of chondrocyte hypertrophy on stress anisotropy. a) Growth of prehypertrophic and hypertrophic chondrocytes depending on the growth constant G. b) Growth plate structure in the No-growth simulation at Day 2; here, the view of the $y = 50$ μm plane of half of the tissue is shown. c) Distribution of stress in radial (σ_r), circumferential (σ_θ), and bone longitudinal (σ_z) directions at Day 2 in the No-growth simulation. d) Stress in radial (σ_r), circumferential (σ_θ), and bone longitudinal (σ_z) directions of proliferative cells at Day 2 depending on the growth constant G. e) Relation between maximum (σ_{max}) and minimum (σ_{min}) principal stress of proliferative cells at Day 2 in the Normal and No-growth simulations. Representative deformation states of cells are shown by yellow ellipses. Scale bar: 100 μm. (For interpretation of the references to color in this figure legend, the reader is referred to the web version of this article.)

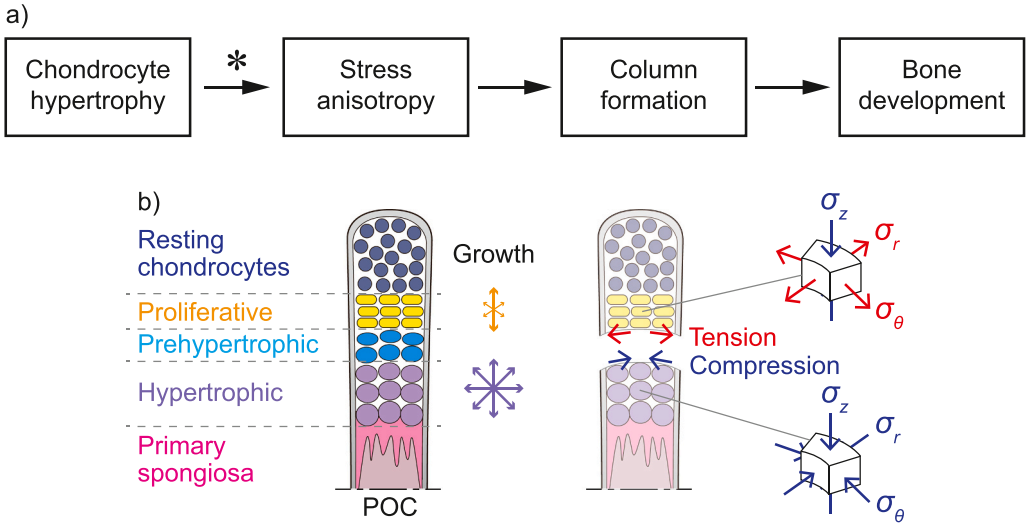

Fig. 6. Proposed mechanism of longitudinal bone growth. a) Chondrocyte hypertrophy promotes stress anisotropy in the proliferative zone, which affects bone development through chondrocyte column formation. b) Mechanics connecting chondrocyte hypertrophy to stress anisotropy in the proliferative zone (* in (a)). Difference in growth rate in the transverse plane between the proliferative and hypertrophic zones induces tension exerted on the proliferative zone and compression exerted on the hypertrophic zone. The proliferative zone is stretched in the transverse plane by the rapidly growing hypertrophic zone. In contrast, the hypertrophic zone is restricted in its growth by the proliferative zone.

phenomena in the development and homeostasis of various multicellular tissues.

The mechanism of longitudinal bone growth (Fig. 6a), which was examined by modeling the mouse metatarsal from E14 to E18 in this study, can be generalized to many types of long bones in various species. The multicellular dynamics observed in this time frame, i.e. from the onset of POC formation to the formation and maintenance of the growth plate, are common in long bones despite diversities in the subsequent timings and positions of SOC formation associated with the variety of shapes of the epiphysis. For example, the period from E16.5 to P5.5 for the mouse femur [36,43] and from 62 days after fertilization to some months after birth for the human femur [44,45] correspond to the time frame from POC formation to SOC formation. During these time frames, each bone can be estimated to grow by a similar mechanism as in this study. Therefore, the mechanism of longitudinal bone growth suggested in this study can be an important mechanism common among these various bones.

The in-plane tension in the proliferative zone disappeared in the No-growth simulation without chondrocyte hypertrophy (Figs. 5c and d). This result suggests that the in-plane tension is caused by the differential growth of the tissue [46]. When only one tissue (A) grows out of two adhered tissues (A and B), the other (B) is stretched by A, whereas A is constrained by B and restricted in its growth. This differential growth occurs between the epiphysis including the proliferative zone and the diaphysis including the hypertrophic zone (Fig. 6b). In the Normal simulation, proliferative cells in the epiphysis mainly grew in the z-direction and did not grow much in the transverse plane, because the direction of division $\boldsymbol{n}_s$ was close to the z-direction (Figs. 1b-1 and 3c). On the other hand, the hypertrophic zone in the diaphysis grew rapidly and isotropically. Accordingly, the difference in the growth rates in the transverse plane in the proliferative and hypertrophic zones led to mechanical interactions between these zones, where the proliferative zone was stretched by the hypertrophic zone, whereas the hypertrophic zone was restricted in its growth by the proliferative zone in the transverse plane (Fig. 6b). The distribution of the in-plane stress (σ_r and σ_θ) in the Normal simulation (Fig. 3d), which varied acutely along the bone longitudinal direction from negative (compressive) in the hypertrophic zone to positive (tensile) in the proliferative zone, supports this assumption. Thus, the spatial distribution of different cell activities, depending on the layered structure of the growth plate, is suggested to be the cause of in-plane tension in the proliferative zone (Fig. 6b). Therefore, this study suggests the importance of growth plate structure in promoting stress anisotropy.

Numerous signaling molecules and other biological factors necessary for chondrocyte column formation in the proliferative zone have been elucidated in previous studies; these include Wnt, N-cadherin, integrin-linked kinase, Rac1, and frizzled [7,9,47–49]. However, the mechanisms by which such signaling molecules cooperate to achieve cell rearrangement after division remain unclear. In this study, as a possible mechanism connecting signaling molecules to changes in cell morphology, the hypothesis [31–34] of energy due to membrane elasticity and adhesion was introduced into the models by assuming that cells align in the most compressive direction of the parent cell, that is, the minimum principal stress direction (Fig. 3e). The simulation based on this assumption for individual cell activities confirmed the chondrocyte column formation along the bone longitudinal axis at the tissue level (Fig. 3c), despite the cells having no information regarding the global longitudinal direction of the bone and there being no other assumption in our model to align the cells or compress them in an arbitrary direction. This result indicates that cell alignment along the most compressive direction is a reasonable mechanism for column formation in growth plates. Nevertheless, some rare cases were also observed, where daughter cells aligned independently of the cell shape in a previous study [6]. This observation implies that additional factors affect the mechanism of cell rearrangement, such as the turnover rate of the membrane and the production of adhesion molecules, depending on the signaling molecules. The effect of such additional factors on cell rearrangement may be elucidated by comparing the cell activities between observations [6] and our simulation.

A limitation of our cell alignment model is the lack of random effects due to fluctuations in cellular behaviors. In our model, the cell alignment axis after division was rigorously determined to be the most compressive direction of the cell, that is, the minimal principal stress direction (Fig. 1b-1). Owing to this excessively sensitive assumption of stress anisotropy, the proliferative cells still formed columns (Fig. S5a) in the No-growth simulation described in Section 3.4, even though the stress anisotropy was small (Fig. 5e). Additionally, the stress in the bone longitudinal direction (σ_z) in most parts of the proliferative zone was more compressive than that in other directions (Figs. 5c and d) in the No-growth simulation. This stress field was derived from a long bone shape independent of the growth plate structure (Section S6). However, if the stress anisotropy is small, as is the case for the No-growth simulation, column formation can be impaired by fluctuations in cellular behaviors. Therefore, chondrocyte hypertrophy's role in promoting stress anisotropy becomes crucial in the mechanism of column formation, considering fluctuations.

This study focused on longitudinal bone growth in the embryonic stages by ignoring the effects of external forces exerted on the bone and by modeling a mouse third metatarsal, owing to its simple and axisymmetric shape. In the embryonic stages, the joint loading and muscle contraction forces exerted on the bone are much smaller than in adults. Certain maternal movements can also causes random forces to parts of the bones. Based on the assumption that the effects of such uncertain external forces are sufficiently small compared to the effects of persistent internal forces caused by chondrocyte activities, we investigated the role of internal forces in bone development by ignoring any such external forces. On the other hand, at later developmental stages, the developmental mechanisms of complex shapes, such as the large convex femoral head and concave neck, are also unknown. Cell dynamics that produce such complex shapes can be investigated in the future by extending our models to simulate the mechanical interactions between tissues, such as the force exerted on a bone by muscles. This extension can enable the description of entire bone morphogenesis and the evaluation of bone mechanical functions, such as load-bearing and body motion, throughout the developmental stages.

Investigation of the spatial distribution of the stress field is difficult within the bone tissue of intact embryos *in vivo*, despite its importance for understanding the regulation mechanism of multicellular dynamics. Actually, measurement of the stress field within tissues in previous studies is limited to estimation of in-plane tension in two-dimensional epithelial tissues by laser ablation [50], measurement of the stress field using microdroplets embedded in embryonic tissues [51], and so on. However, although the validation of the stress field results is outside the scope of this study, the simulation platform developed here based on CbPM enabled stress analysis within the growing tissue and revealed that chondrocyte hypertrophy promotes stress anisotropy in the proliferative zone of the growth plate. Stress anisotropy has been suggested to affect bone development via chondrocyte column formation. The stress field specific to each growth plate zone observed in this study may also play a role in regulating other cellular activities, such as differentiation. Therefore, the stress analysis enabled by the multicellular simulation platform developed in this study provide further insight into the mechanical regulation of multicellular dynamics within developing bone tissue. Moreover, extending the simulation platform by modeling the mechanical interaction between tissues can enable the investigation of the mechanical behaviors of a wide range of biological tissues throughout the developmental stages.

CRediT authorship contribution statement

Yuka Yokoyama: Writing – review & editing, Writing – original draft, Visualization, Validation, Software, Resources, Methodology,

Investigation, Funding acquisition, Formal analysis, Data curation, Conceptualization. **Yoshitaka Kameo:** Writing – review & editing, Resources, Funding acquisition, Conceptualization. **Junko Sunaga:** Writing – review & editing, Visualization, Data curation. **Koichiro Maki:** Writing – review & editing, Resources. **Taiji Adachi:** Writing – review & editing, Supervision, Resources, Project administration, Funding acquisition, Conceptualization.

Declaration of competing interest

The authors declare that they have no known competing financial interests or personal relationships that could have appeared to influence the work reported in this paper.

Data availability

Data will be made available on request.

Acknowledgments

Funding: This work was supported by Grant-in-Aid for JSPS Fellows (JP23KJ1234) and Grant-in-Aid for Scientific Research (A) (JP20H00659) and (C) (JP22K03827) from the Japan Society for the Promotion of Science (JSPS); JST-CREST (JPMJCR22L5); JST FOREST Program (JPMJFR222D); and Mori Manufacturing Research and Technology Foundation.

Appendix A. Supplementary data

Supplementary data to this article can be found online at https://doi.org/10.1016/j.bone.2024.117055.

References

[1] H.M. Kronenberg, Developmental regulation of the growth plate, Nature 423 (2003) 332–336, https://doi.org/10.1038/nature01657.
[2] G.L. Galea, M.R. Zein, S. Allen, P. Francis-West, Making and shaping endochondral and intramembranous bones, Dev. Dyn. 250 (2021) 414–449, https://doi.org/10.1002/dvdy.278.
[3] J.C. Nguyen, B.K. Markhardt, A.C. Merrow, J.R. Dwek, Imaging of pediatric growth plate disturbances, RadioGraphics 37 (2017) 1791–1812, https://doi.org/10.1148/rg.2017170029.
[4] E. Kozhemyakina, A.B. Lassar, E. Zelzer, A pathway to bone: signaling molecules and transcription factors involved in chondrocyte development and maturation, Development 142 (2015) 817–831, https://doi.org/10.1242/dev.105536.
[5] S. Provot, E. Schipani, Molecular mechanisms of endochondral bone development, Biochem. Biophys. Res. Commun. 328 (2005) 658–665, https://doi.org/10.1016/j.bbrc.2004.11.068.
[6] S.M. Romereim, N.H. Conoan, B. Chen, A.T. Dudley, A dynamic cell adhesion surface regulates tissue architecture in growth plate cartilage, Development 141 (2014) 2085–2095, https://doi.org/10.1242/dev.105452.
[7] Y. Li, A.T. Dudley, Noncanonical frizzled signaling regulates cell polarity of growth plate chondrocytes, Development 136 (2009) 1083–1092, https://doi.org/10.1242/dev.023820.
[8] A. Aszodi, E.B. Hunziker, C. Brakebusch, R. Fässler, β1 integrins regulate chondrocyte rotation, G1 progression, and cytokinesis, Genes Dev. 17 (2003) 2465–2479, https://doi.org/10.1101/gad.277003.
[9] Y. Li, A. Li, J. Junge, M. Bronner, Planar cell polarity signaling coordinates oriented cell division and cell rearrangement in clonally expanding growth plate cartilage, ELife 6 (2017) e23279, https://doi.org/10.7554/eLife.23279.
[10] B. St-Jacques, M. Hammerschmidt, A.P. McMahon, Indian hedgehog signaling regulates proliferation and differentiation of chondrocytes and is essential for bone formation, Genes Dev. 13 (1999) 2072–2086, https://doi.org/10.1101/gad.13.16.2072.
[11] A. Vortkamp, K. Lee, B. Lanske, G.V. Segre, H.M. Kronenberg, C.J. Tabin, Regulation of rate of cartilage differentiation by Indian hedgehog and PTH-related protein, Science 273 (1996) 613–622, https://doi.org/10.1126/science.273.5275.613.
[12] F. Long, U. Chung, S. Ohba, J. McMahon, H.M. Kronenberg, A.P. McMahon, Ihh signaling is directly required for the osteoblast lineage in the endochondral skeleton, Development 131 (2004) 1309–1318, https://doi.org/10.1242/dev.01006.
[13] Q. Wu, Y. Zhang, Q. Chen, Indian hedgehog is an essential component of Mechanotransduction complex to stimulate chondrocyte proliferation *, J. Biol. Chem. 276 (2001) 35290–35296, https://doi.org/10.1074/jbc.M101055200.
[14] N. Felsenthal, E. Zelzer, Mechanical regulation of musculoskeletal system development, Development 144 (2017) 4271–4283, https://doi.org/10.1242/dev.151266.
[15] A.S. Pollard, B.G. Charlton, J.R. Hutchinson, T. Gustafsson, I.M. McGonnell, J. A. Timmons, A.A. Pitsillides, Limb proportions show developmental plasticity in response to embryo movement, Sci. Rep. 7 (2017) 41926, https://doi.org/10.1038/srep41926.
[16] J.M. Collins, A. Lang, C. Parisi, Y. Moharrer, M.P. Nijsure, J.H. (Thomas) Kim, G. L. Szeto, L. Qin, R. Gottardi, N. Dyment, N. Nowlan, J.D. Boerckel, YAP and TAZ couple osteoblast precursor mobilization to angiogenesis and mechanoregulated bone development, Dev. Biol. (2023), https://doi.org/10.1101/2023.01.20.524918.
[17] Y. Shwartz, Z. Farkas, T. Stern, A. Aszódi, E. Zelzer, Muscle contraction controls skeletal morphogenesis through regulation of chondrocyte convergent extension, Dev. Biol. 370 (2012) 154–163, https://doi.org/10.1016/j.ydbio.2012.07.026.
[18] Y. Yokoyama, Y. Kameo, T. Adachi, Development of continuum-based particle models of cell growth and proliferation for simulating tissue morphogenesis, J. Mech. Behav. Biomed. Mater. 142 (2023) 105828, https://doi.org/10.1016/j.jmbbm.2023.105828.
[19] T. Kawamoto, K. Kawamoto, Preparation of thin frozen sections from nonfixed and Undecalcified hard tissues using Kawamoto's film method (2020), in: M.J. Hilton (Ed.), Skeletal Development and Repair: Methods and Protocols, Springer US, New York, NY, 2021, pp. 259–281, https://doi.org/10.1007/978-1-0716-1028-2_15.
[20] T. Kawamoto, Use of a new adhesive film for the preparation of multi-purpose fresh-frozen sections from hard tissues, whole-animals, insects and plants, Arch. Histol. Cytol. 66 (2003) 123–143, https://doi.org/10.1679/aohc.66.123.
[21] D. Studer, C. Millan, E. Oeztuerk, K. Maniura-Weber, M. Zenobi-Wong, Molecular and biophysical mechanisms regulating hypertrophic differentiation in chondrocytes and mesenchymal stem cells, Eur. Cells Mater. 24 (2012) 118–135, https://doi.org/10.22203/eCM.v024a09.
[22] C.E. Farnum, M. Tinsley, J.W. Hermanson, Forelimb versus Hindlimb skeletal development in the big brown bat, *Eptesicus fuscus*: Functional divergence is reflected in chondrocytic performance in autopodial growth plates, CTO 187 (2008) 35–47, https://doi.org/10.1159/000109962.
[23] J.D. Green, V. Tollemar, M. Dougherty, Z. Yan, L. Yin, J. Ye, Z. Collier, M. K. Mohammed, R.C. Haydon, H.H. Luu, R. Kang, M.J. Lee, S.H. Ho, T.-C. He, L. L. Shi, A. Athiviraham, Multifaceted signaling regulators of chondrogenesis: implications in cartilage regeneration and tissue engineering, Genes & Diseases 2 (2015) 307–327, https://doi.org/10.1016/j.gendis.2015.09.003.
[24] C.J. Philpott, N.A. Rahman, N. Kenny, T.R. Londo, R.M. Young, B. George Barisas, D.A. Roess, Rotational dynamics of luteinizing hormone receptors and MHC class I antigens on murine Leydig cells, Biochim. Biophys. Acta Biomembr. 1235 (1995) 62–68, https://doi.org/10.1016/0005-2736(94)00277-V.
[25] S. Basu, P.J. Campagnola, Properties of crosslinked protein matrices for tissue engineering applications synthesized by multiphoton excitation, J. Biomed. Mater. Res. A 71A (2004) 359–368, https://doi.org/10.1002/jbm.a.30175.
[26] D.A. Garzón-Alvarado, J.M. García-Aznar, M. Doblaré, A reaction–diffusion model for long bones growth, Biomech. Model. Mechanobiol. 8 (2009) 381–395, https://doi.org/10.1007/s10237-008-0144-z.
[27] P.L. Reno, D.L. Mcburney, C.O. Lovejoy, W.E. Horton Jr., Ossification of the mouse metatarsal: differentiation and proliferation in the presence/absence of a defined growth plate, Anat. Rec. A Discov. Mol. Cell. Evol. Biol. 288A (2006) 104–118, https://doi.org/10.1002/ar.a.20268.
[28] G. Himpel, E. Kuhl, A. Menzel, P. Steinmann, Computational modelling of isotropic multiplicative growth, Computer Modeling in Engineering & Sciences 8 (2005) 119–134, https://doi.org/10.3970/cmes.2005.008.119.
[29] H. Takeda, Y. Kameo, Y. Inoue, T. Adachi, An energy landscape approach to understanding variety and robustness in tissue morphogenesis, Biomech. Model. Mechanobiol. 19 (2020) 471–479, https://doi.org/10.1007/s10237-019-01222-5.
[30] R. de Rooij, E. Kuhl, A physical multifield model predicts the development of volume and structure in the human brain, J. Mech. Phys. Solids 112 (2018) 563–576, https://doi.org/10.1016/j.jmps.2017.12.011.
[31] S. Hilgenfeldt, S. Erisken, R.W. Carthew, Physical modeling of cell geometric order in an epithelial tissue, Proc. Natl. Acad. Sci. 105 (2008) 907–911, https://doi.org/10.1073/pnas.0711077105.
[32] I.M. Gemp, R.W. Carthew, S. Hilgenfeldt, Cadherin-dependent cell morphology in an epithelium: constructing a quantitative dynamical model, PLoS Comput. Biol. 7 (2011) e1002115, https://doi.org/10.1371/journal.pcbi.1002115.
[33] T. Hayashi, R.W. Carthew, Surface mechanics mediate pattern formation in the developing retina, Nature 431 (2004) 647–652, https://doi.org/10.1038/nature02952.
[34] A.N. Malmi-Kakkada, S. Sinha, X. Li, D. Thirumalai, Adhesion strength between cells regulate nonmonotonic growth by a biomechanical feedback mechanism, Biophys. J. 121 (2022) 3719–3729, https://doi.org/10.1016/j.bpj.2022.04.032.
[35] N.J. Wilsman, C.E. Farnum, E.M. Green, E.M. Lieferman, M.K. Clayton, Cell cycle analysis of proliferative zone chondrocytes in growth plates elongating at different rates, J. Orthop. Res. 14 (1996) 562–572, https://doi.org/10.1002/jor.1100140410.
[36] E.S. Hara, M. Okada, N. Nagaoka, T. Hattori, L.M. Iida, T. Kuboki, T. Nakano, T. Matsumoto, Chondrocyte burst promotes space for mineral expansion, Integr. Biol. 10 (2018) 57–66, https://doi.org/10.1039/C7IB00130D.
[37] S. Rubin, A. Agrawal, J. Stegmaier, S. Krief, N. Felsenthal, J. Svorai, Y. Addadi, P. Villoutreix, T. Stern, E. Zelzer, Application of 3D MAPs pipeline identifies the morphological sequence chondrocytes undergo and the regulatory role of GDF5 in this process, Nat. Commun. 12 (2021) 5363, https://doi.org/10.1038/s41467-021-25714-0.

[38] Q. Luo, D. Kuang, B. Zhang, G. Song, Cell stiffness determined by atomic force microscopy and its correlation with cell motility, Biochim. Biophys. Acta Gen. Subj. 1860 (2016) 1953–1960, https://doi.org/10.1016/j.bbagen.2016.06.010.
[39] W.R. Trickey, F.P.T. Baaijens, T.A. Laursen, L.G. Alexopoulos, F. Guilak, Determination of the Poisson's ratio of the cell: recovery properties of chondrocytes after release from complete micropipette aspiration, J. Biomech. 39 (2006) 78–87, https://doi.org/10.1016/j.jbiomech.2004.11.006.
[40] R.M. Pidaparti, A. Vogt, Experimental investigation of Poisson's ratio as a damage parameter for bone fatigue, J. Biomed. Mater. Res. 59 (2002) 282–287, https://doi.org/10.1002/jbm.1243.
[41] J.J. Vaca-González, M. Moncayo-Donoso, J.M. Guevara, Y. Hata, S.J. Shefelbine, D. A. Garzón-Alvarado, Mechanobiological modeling of endochondral ossification: an experimental and computational analysis, Biomech. Model. Mechanobiol. 17 (2018) 853–875, https://doi.org/10.1007/s10237-017-0997-0.
[42] S.M. Sadeghian, F.D. Shapiro, S.J. Shefelbine, Computational model of endochondral ossification: simulating growth of a long bone, Bone 153 (2021) 116132, https://doi.org/10.1016/j.bone.2021.116132.
[43] M. Moncayo-Donoso, J.M. Guevara, K. Márquez-Flórez, M.R. Fontanilla, L. A. Barrera, D.A. Garzón-Alvarado, Morphological changes of physeal cartilage and secondary ossification centres in the developing femur of the house mouse (*Mus musculus*): a micro-CT based study, Anat. Histol. Embryol. 48 (2019) 117–124, https://doi.org/10.1111/ahe.12417.
[44] Y. Suzuki, J. Matsubayashi, X. Ji, S. Yamada, A. Yoneyama, H. Imai, T. Matsuda, T. Aoyama, T. Takakuwa, Morphogenesis of the femur at different stages of normal human development, PloS One 14 (2019) e0221569, https://doi.org/10.1371/journal.pone.0221569.
[45] C. Hansman, Appearance and fusion of ossification centers in human skeleton, American Journal of Roentgenology Radium Therapy and Nuclear Medicine 88 (1962) 476–482.
[46] C. Huang, Z. Wang, D. Quinn, S. Suresh, K.J. Hsia, Differential growth and shape formation in plant organs, Proc. Natl. Acad. Sci. 115 (2018) 12359–12364, https://doi.org/10.1073/pnas.1811296115.
[47] B. Gao, H. Song, K. Bishop, G. Elliot, L. Garrett, M.A. English, P. Andre, J. Robinson, R. Sood, Y. Minami, A.N. Economides, Y. Yang, Wnt signaling gradients establish planar cell polarity by inducing Vangl2 phosphorylation through Ror2, Dev. Cell 20 (2011) 163–176, https://doi.org/10.1016/j.devcel.2011.01.001.
[48] C. Grashoff, A. Aszódi, T. Sakai, E.B. Hunziker, R. Fässler, Integrin-linked kinase regulates chondrocyte shape and proliferation, EMBO Rep. 4 (2003) 432–438, https://doi.org/10.1038/sj.embor.embor801.
[49] G. Wang, A. Woods, H. Agoston, V. Ulici, M. Glogauer, F. Beier, Genetic ablation of Rac1 in cartilage results in chondrodysplasia, Dev. Biol. 306 (2007) 612–623, https://doi.org/10.1016/j.ydbio.2007.03.520.
[50] R.M. Herrera-Perez, C. Cupo, C. Allan, A.B. Dagle, K.E. Kasza, Tissue flows are tuned by actomyosin-dependent mechanics in developing embryos, PRX Life 1 (2023) 013004, https://doi.org/10.1103/PRXLife.1.013004.
[51] O. Campàs, T. Mammoto, S. Hasso, R.A. Sperling, D. O'Connell, A.G. Bischof, R. Maas, D.A. Weitz, L. Mahadevan, D.E. Ingber, Quantifying cell-generated mechanical forces within living embryonic tissues, Nat. Methods 11 (2014) 183–189, https://doi.org/10.1038/nmeth.2761.